*Inorg. Chem.* **2004**, *43*, 7339–7345


# Size and Surface Effects of Prussian Blue Nanoparticles Protected by Organic Polymers

**Takashi Uemura, Masaaki Ohba, and Susumu Kitagawa***

*Department of Synthetic Chemistry and Biological Chemistry, Graduate School of Engineering, Kyoto University, Katsura, Nishikyo-ku, Kyoto 615-8510, Japan*

Received August 23, 2004

Prussian blue (PB) nanoparticles protected by organic polymers such as poly(vinylpyrrolidone) (PVP) and poly(diallyldimethylammonium chloride) (PDDA) were prepared. Different experimental conditions (concentrations of Fe ions and feed ratios of Fe to the polymers) have been investigated to control the size of the PB nanoparticles. For example, the averaged dimensions of the PB nanoparticles were tuned from 12 to 27 nm by use of PVP in the different conditions. Addition of PDDA produced the PB nanoparticles with very small dimensions (5–8 nm) by an effective electrostatic interaction. We found that the surface environments of the PB nanoparticles affect the inherent properties of PB. The shifts of charge transfer (CT) absorptions from $Fe^{2+}$ to $Fe^{3+}$ in the PB nanoparticles resulted from the surface-protecting polymers. Especially, the PB nanoparticles with the PVP protection show high solubility in a variety of organic solvents and a solvent-dependent CT absorption. Measurement of the magnetic properties of the PB nanoparticles showed unprecedented size-dependency, surface effect, and superparamagnetic properties.

## Introduction

Tremendous attention has been paid to inorganic nanosize crystals in recent years because of their significant properties determined by the high surface areas and quantization of most electronic properties.[1] Especially, nanosize magnetic materials have been intensively studied as essential elements in future spintronics due to the application to ultrahigh-density magnetic recording devices.[2] In the nanometer size regime, the crystal size of the magnetic particles is a key factor that governs their magnetic properties. Monodisperse nanocrystals composed of Fe,[3] Co,[4] $CoPt_3$,[5] and FePt[6] with controlled sizes have been successfully synthesized with the aim of understanding the influence of their sizes on the magnetic behaviors.

Prussian blue (PB) analogues $M_i^{m+}[M'(CN)_6]^{n-}$ have played important roles in the field of molecule-based magnets.[7] One of the most interesting aspects of these materials is a designable and controllable magnetic property by tuning type, ratio, and combination of metal ions incorporated as spin centers in the structures. The versatile superexchange interactions between the neighboring metal ions through the cyanide bridges afford them unique magnetic properties. For instance, Verdaguer's groups have prepared a new PB derivative presenting a magnetic ordering at transition temperature as high as 315 K.[7b] Photomagnetic

* To whom correspondence should be addressed. E-mail: kitagawa@sbchem.kyoto-u.ac.jp.

(1) (a) *Clusters and Colloids*; Schmid, G., Ed.; VCH: Weinheim, 1994. (b) Alivisatos, A. P. *Science* **1996**, *271*, 933. (c) Kamat, P. V. *J. Phys. Chem. B* **2002**, *106*, 7729.

(2) (a) Black, C. T.; Murray, C. B.; Sandstrom, R. L.; Sun, S. *Science* **2000**, *290*, 1131. (b) Sun, S.; Murray, C. B.; Weller, D.; Folks, L.; Moser, A. *Science* **2000**, *287*, 1989. (c) Hashimoto, S.; Maesaka, A.; Fujimoto, K.; Bessho, K. *J. Magn. Magn. Mater*. **1993**, *121*, 471.

(3) (a) Suslick, K. S.; Fang, M.; Hyeon, T. *J. Am. Chem. Soc*. **1996**, *118*, 11960. (b) Park, S.-J.; Kim, S.; Lee, S.; Khim, Z.; Char, K.; Hyeon, T. *J. Am. Chem. Soc*. **2000**, *122*, 8581.

(4) (a) Sun, S.; Murray, C. B. *J. Appl. Phys*. **1999**, *85*, 4325. (b) Puntes, V. F.; Krishnan, K. M.; Alivisatos, A. P. *Science* **2001**, *291*, 2115.

(5) (a) Schevchenko, E. V.; Talapin, D. V.; Rogach, A. L.; Kornowski, A.; Haase, M.; Weller, H. *J. Am. Chem. Soc*. **2002**, *124*, 11480. (b) Schevchenko, E. V.; Talapin, D. V.; Schnablegger, H.; Kornowski, A.; Festin, Ö.; Svedlindh, P.; Haase, M.; Weller, H. *J. Am. Chem. Soc*. **2003**, *125*, 9090.

(6) Sun, S.; Murray, C. B.; Weller, D.; Folks, L.; Moser, A. *Science* **2000**, *287*, 1989.

(7) (a) Ohkoshi, S.; Abe, Y.; Fujishima, A.; Hashimoto, K. *Phys. Rev. Lett.* **1999**, *82*, 1285. (b) Ferlay, S.; Mallah, T.; Quahés, R.; Veillet, P.; Verdaguer, M. *Nature* **1995**, *378*, 701. (c) Holmes, H. S.; Girolami, G. S. *J. Am. Chem. Soc*. **1999**, *121*, 5593. (d) Ohkoshi, S.; Iyoda, T.; Fujishima, A.; Hashimoto, K. *Phys. Rev. B* **1997**, *56*, 11642. (e) Buschmann, W. E.; Ensling, J.; Gütlich, P.; Miller, J. S. *Chem. Eur. J.* **1999**, *5*, 3019. (f) Sato, O.; Iyoda, T.; Fujishima, A.; Hashimoto, K. *Science* **1996**, *272*, 704. (g) Tokoro, H.; Ohkoshi, S.; Hashimoto, K. *Appl. Phys. Lett*. **2003**, *82*, 1245. (h) Ohkoshi, S.; Yorozu, S.; Sato, O.; Iyoda, T.; Fujishima, A.; Hashimoto, K. *Appl. Phys. Lett*. **1997**, *70*, 1040. (i) Ito, A.; Suenaga, M.; Ono, K. *J. Chem. Phys*. **1968**, *48*, 3597.

10.1021/ic0488435 CCC: $27.50 
Published on Web 10/13/2004

**Chart 1**

poly(vinylpyrrolidone) (**PVP**)

poly(diallyldimethylammonium chloride) (**PDDA**)

behaviors such as photoinduced magnetization,[7f] photodemagnetization,[7g] and magnetic pole inversion[7h] based on the PB analogues have been reported by Hashimoto's group.

In the past few years, several attempts at syntheses of the PB family nanoparticles have emerged as a promising subject for applications to the nanomagnetic devices.[8] To understand how the properties of the PB derivatives develop as a function of size at the nanometer scale is of fundamental and technological interest. Some reports show superparamagnetic behaviors of the PB derivatives accompanied by the nanosize dimensions of the magnetic crystals.[8d,e] Previously, we reported an initial study on PB nanoparticles with different crystal sizes, which demonstrate the first size-dependent magnetic property of the PB family.[8c]

Functionalized organic polymers have been widely used as substances for the preparation of metal-based nanoparticles.[9] The selection of appropriate protective polymers not only leads to various colloid morphologies by controlling the growth and handling of the agglomeration process but also leads to new attractive properties based on the organic−inorganic hybridizations at nanometer scale. In this paper, we describe an effective approach for synthesis of size-controlled PB nanoparticles by use of organic polymers. We employed poly(vinylpyrrolidone) (PVP) and poly(diallyldimethylammonium chloride) (PDDA) as protecting polymers (Chart 1). PVP has repeating amide moieties that can weakly bind to iron ions through a coordinating interaction. It is expected that positively charged PDDA interacts with a negatively charged PB colloid. The principle is based on the fact that the polymers can interact with growing a PB nucleus in the site-specific way, depending on their functional groups. Here we also demonstrate new and important protecting polymers and size-dependent effects of the PB nanoparticles on optical and magnetic properties.

## Experimental Section

**Materials.** All reagents and chemicals were obtained from commercial sources and used without further purification.

**Synthesis of PB. PB Nanoparticles Protected by PVP.** In a typical synthesis ($Fe^{2+}$, $Fe^{3+}$ = 10 mM, PVP/$Fe^{2+}$ = 20), an aqueous $K_3[Fe(CN)_6]$ (33 mg, 0.10 mmol) solution (2 mL) was slowly added to an aqueous $FeCl_2 \cdot 4H_2O$ (2−20 mg; 0.01−0.10 mmol) and PVP (K-30; average $M_w$ = 40000, 222 mg, 2 mmol) solution (8 mL) at room temperature with a vigorous stirring. After the addition, the reaction mixture turned blue immediately, indicating the formation of PB. In order to obtain a powder sample of a PB-PVP composite, 2.5 mL of acetone was added to 1 mL of the reaction mixture. This process is effective in removing KCl from the composite. The resultant precipitate was centrifuged and washed with acetone several times.

**PB Nanoparticles Protected by PDDA.** PB-PDDA nanocomposites were prepared by repeating the above procedure with substitution of PDDA (purchased from Aldrich; average $M_w$ = 100000−200000) for PVP. Upon mixing, the corresponding solution ($Fe^{2+}$ = $Fe^{3+}$ = 3 mM, PDDA = 300 mM) gradually turned dark blue, indicating the formation of PB. Isolation of a PB-PDDA composite was carried out by an addition of acetone (2 mL) to the PB solution (1 mL). The resultant pastelike precipitate was centrifuged and washed with acetone several times.

**Bulk PB.** Aqueous solution (30 mM) of $K_3[Fe(CN)_6]$ was added to a vigorously stirred 30 mM aqueous solution of $FeCl_2$. The resulting precipitate was filtered and washed with methanol.

**Measurements.** X-ray powder diffraction (XRPD) data were collected on a Rigaku RINT 2000 Ultima diffractometer with Cu Kα radiation. IR spectra were recorded on a Perkin-Elmer 2000 FTIR spectrophotometer with samples prepared as KBr pellets. UV−vis spectroscopy data were obtained by use of a Hitachi U-3500 at room temperature; especially, solid-state UV−vis measurements were conducted with samples prepared as KBr pellets. Transmission electron microscopy (TEM) was performed by use of a Hitachi H-7500 electron microscope at an accelerating voltage of 80 kV. For the TEM observations, sample solutions were kept for 7−10 days without stirring. Several drops of the solution were placed on a 200 mesh copper grid covered with a carbon film. Excess solutions were removed with filter paper. The resultant grid was dried in air for 5 h. The mean diameters were calculated by counting 100 particles from the TEM photographs. A prolonged exposure of the electron beam over 5 min seriously damaged the samples. Alternating current (ac) and direct current (dc) magnetic susceptibilities were measured on a Quantum Design MPMS-%XL SQUID susceptometer in the temperature range 2−30 K.

## Results and Discussion

**1. Formations of PB Nanoparticles Protected by Organic Polymers.** In the first set of experiments, the effect of PVP (K-30; average $M_w$ = 40000) on the formation of PB nanoparticles was confirmed. Equimolar amounts of aqueous $FeCl_2$ and $K_3Fe(CN)_6$ solutions were mixed in the presence of PVP with changing concentrations ([$Fe^{2+}$] = [$Fe^{3+}$] = 1−10 mM, [PVP] = 10−1000 mM). Upon mixing, all the solutions immediately turned dark blue, indicating the formation of PB. The absorption spectra of the resulting solutions revealed a peak around 690 nm, which is attributed to an intermetal charge transfer (CT) band from $Fe^{2+}$ to $Fe^{3+}$ of PB.[10] TEM images of these samples after being air-dried on the TEM copper grids show formation of spherical nanoparticles without particles aggregations (Figure 1a−d), suggesting that PVP stabilized the PB nanoparticles and prevented the further aggregation of the particles. The mean

(8) (a) Vaucher, S.; Li, M.; Mann, S. *Angew. Chem., Int. Ed.* **2000**, *39*, 1793. (b) Vaucher, S.; Fielden, J.; Li, M.; Dujardin, E.; Mann, S. *Nano Lett.* **2002**, *2*, 225. (c) Uemura, T.; Kitagawa, S. *J. Am. Chem. Soc.* **2003**, *125*, 7814. (d) Catala, L.; Gacoin, T.; Boilot, J.-P.; Rivière, É.; Paulsen, C.; Lhotel, E.; Mallah, T. *Adv. Mater.* **2003**, *15*, 826. (e) Moore, J. G.; Lochner, E. J.; Ramsey, C.; Dalal, N. S.; Stiegman, A. E. *Angew. Chem., Int. Ed.* **2003**, *42*, 2741. (f) Dominguez-Vera, J. M.; Colacio, E. *Inorg. Chem.* **2003**, *42*, 6983.

(9) (a) *Nanoparticles and Nanostructured Films*; Fendler, J. H., Ed.; Wiley-VCH: Weinheim, 1998. (b) Mayer, A.; Antonietti, M. *Colloid Polym. Sci.* **1998**, *276*, 769.

(10) Robin, M. B. *Inorg. Chem.* **1962**, *1*, 337.

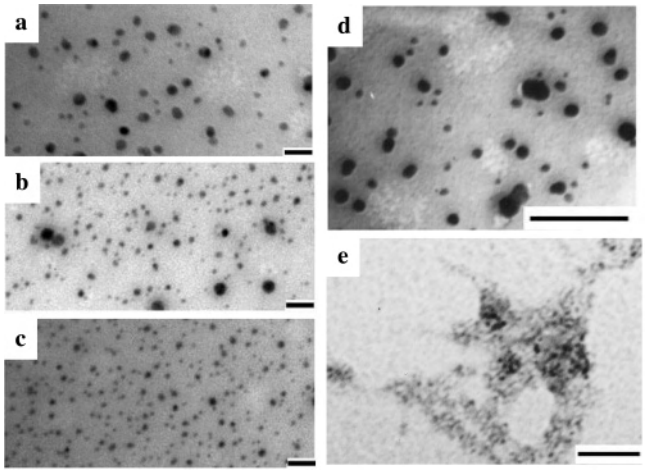


**Figure 1.** TEM images of PVP-protected PB nanoparticles prepared at $[Fe^{2+}] = [Fe^{3+}] = 10$ mM, $[PVP]/[Fe^{2+}] =$ (a) 20, (b) 50, and (c) 100. (d) PVP-protected PB nanoparticles obatined at $[Fe^{2+}] = [Fe^{3+}] = 1$ mM. $[PVP]/[Fe^{2+}] = 100$. (e) PDDA-protected PB nanoparticles at the condition of $[Fe^{2+}] = [Fe^{3+}] = 3$ mM. $[PDDA]/[Fe^{2+}] = 100$. Scale bars in all figures = 100 nm.

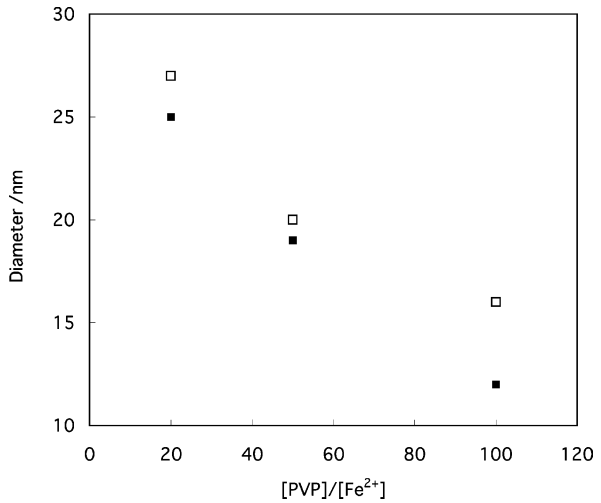


**Figure 2.** Influence of $[PVP]/[Fe^{2+}]$ feed ratio on the average size of PB-PVP*x*; □, $[Fe^{2+}] = 10$ mM; ■, $[Fe^{2+}] = 1$ mM.

diameters of the resultant particles ranged from 12 to 27 nm, depending on the reaction conditions. The averaged diameter of the nanoparticles versus the $[PVP]/[Fe^{2+}]$ ratio plot is shown in Figure 2. As is seen in the profile, the diameters of the nanoparticles became smaller with increase of the PVP content at constant Fe concentrations. The higher concentration of PVP is expected to suppress the crystal growth of PB to yield the smaller nanoparticles. It is also observed that initial Fe ion concentration influenced the particle size. At lower concentrations of initial Fe ions, the final particle size became relatively smaller. Here we abbreviate the PVP protected PB nanoparticles with *x* nm of the averaged diameter to PB-PVP*x*.

Figure 3 shows the XRPD pattern for PB-PVP27 and bulk PB whose particle size is over 500 nm determined from a TEM image. All the diffraction peaks of PB-PVP27 appeared at same positions of those for the bulk PB, which was indexed to the cubic space group *Fm*3*m*.[11] From the width of the diffraction peaks using Sherrer's law, the average size

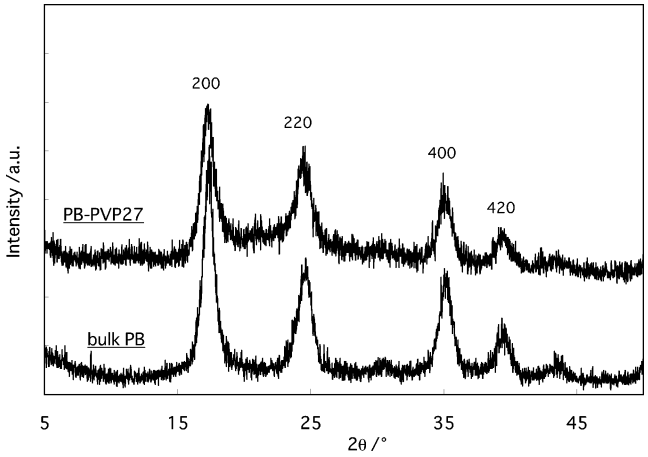


**Figure 3.** XRPD patterns of PB-PVP27 and bulk PB.

of the crystalline domains for PB-PVP27 as well as the bulk PB can be estimated to be almost the same (about 8 nm), which is inconsistent with the results from the TEM experiment. Similar results were obtained by use of the other PB-PVP*x* species. In the usual synthesis of the PB analogues, alkali ions are incorporated in lattice defects (incomplete coordinated $M(CN)_6$ sites) of the PB frameworks. In order to evaluate the crystallinity of PB-PVP*x*, inductively coupled plasma mass spectral (ICP-MS) analyses for determinations of the composition ratios of iron to potassium ions were performed. The values of Fe/K for PB-PVP*x* by the ICP-MS analysis are $2.8 \pm 0.3$ independent of the particle size,[12] indicating that all PB-PVP*x* species contain the lattice defects with a constant ratio in the structures. Therefore, the smaller crystalline domain sizes of the PB-PVP*x* and bulk PB calculated from the XRPD results are caused by the existence of such defect sites in the frameworks. The IR spectrum of PB-PVP27 in the 2000−2200 $cm^{-1}$ region showed a strong band at 2086 $cm^{-1}$ associated with CN stretching in the $Fe^{2+}-CN-Fe^{3+}$ of PB (Figure 4). The spectrum also showed a peak for C═O stretching of the PVP amide unit at 1656 $cm^{-1}$ together with a shoulder peak around 1600 $cm^{-1}$. The appearance of the latter shoulder peak suggested a part of amide unit in PVP binds to the Fe ions of PB. These results indicate that, during nucleation and growth processes of PB, the amide moieties of PVP weakly coordinated to Fe ions; consequently, PVP provided steric stabilization.

We studied as well the influence of cationic PDDA on the nanoparticle formation of PB by the experiments with varying the concentrations and ratios of the Fe ions and PDDA ($[Fe^{2+}] = [Fe^{3+}] = 1-10$ mM, $[PDDA] = 10-500$ mM). Compared to the PVP system, the reaction time apparently increased, indicating that the strong electrostatic interaction between cationic PDDA and $Fe(CN)_6^{3-}$ decreases the rate of nucleation for PB. It takes about 4 days to complete the formation of PB in all cases. Particularly, PB

(11) Buser, H. J.; Schwarzenbach, D.; Petter, W.; Ludi, A. *Inorg. Chem.* **1977**, *16*, 2704.

(12) ICP-MS results (wt %) for PB-PVP27: Fe, 11.29; K, 2.63. PB-PVP20: Fe, 4.83; K, 1.33. PB-PVP16: Fe, 3.04; K, 0.78. PB-PVP12: Fe, 12.69; K, 3.16. PB-PDDA (prepared condition: $[Fe^{2+}] = [Fe^{3+}] = 3$ mM, $[PDDA]/[Fe^{2+}] = 100$): Fe, 2.64; K, 0.10.

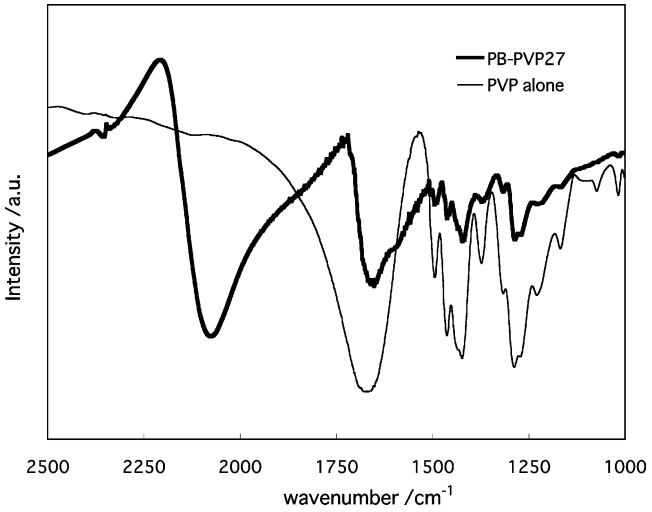


**Figure 4.** IR spectra of PB-PVP27 and PVP alone.

did not form at the $Fe^{2+}$ concentration of 1 mM when the ratio of [PDDA]/[$Fe^{2+}$] is more than 5, which is confirmed by the UV−vis absorption change. Due to the slow reaction rates, we kept the reaction mixtures for at least 10 days before the TEM measurement. The TEM images showed a different trend compared to those observed for the PVP system (Figure 1e); that is, the feed ratio and concentration of the Fe ions and PDDA did not affect the average size of the nanoparticles. In every experiment, very small nanoparticles with diameters of 5−8 nm were always obtained as dispersed forms in the PDDA matrix. The full characterizations by XRPD, UV−vis, IR, and ICP-MS measurements support the products as PB nanoparticles protected by PDDA (PB-PDDA).[12,13] The crystal size of PB-PDDA was estimated to be 7.1 nm from Sherrer's equation for the XRPD pattern, which fits the grain size of the TEM image well. This result indicates the structure of PB-PDDA with fewer defects. The remarkable decrease of the particle size compared with those of PB-PVP*x* is ascribed to suppression of the crystal growth by the effective electrostatic interaction between cationic PDDA and the negatively charged PB colloid.

**2. Optical Properties of the PB Nanoparticles.** The UV−vis absorptions of PB-PVP12, PB-PDDA, and bulk PB in aqueous solutions are seen in Figure 5a. The maximum peak due to the $Fe^{II}$ to $Fe^{III}$ CT of PB-PVP12 (689 nm) was located at a shorter wavelength than that of the bulk PB (700 nm). In the case of PB-PDDA, the peak shifted to longer wavelength (724 nm) by 24 nm from that of the bulk PB. In addition, absorptions of PB-PVP12 and PB-PDDA in the solid state gave larger adsorption shifts (Figure 5b) due to the stronger interaction between the surface polymers and the inner PB particles. The difference in the color between PB-PVP12 and PB-PDDA could be distinguished (PB-PVP12, vivid blue; PB-PDDA, subdued blue). These results indicate that the surface protecting polymers significantly affect the Coulombic energy expended in transferring the electron from $Fe^{II}$ to $Fe^{III}$ in the nanoparticles.[10,14] It is also reported that the PB intercalated in bilayer films exhibited

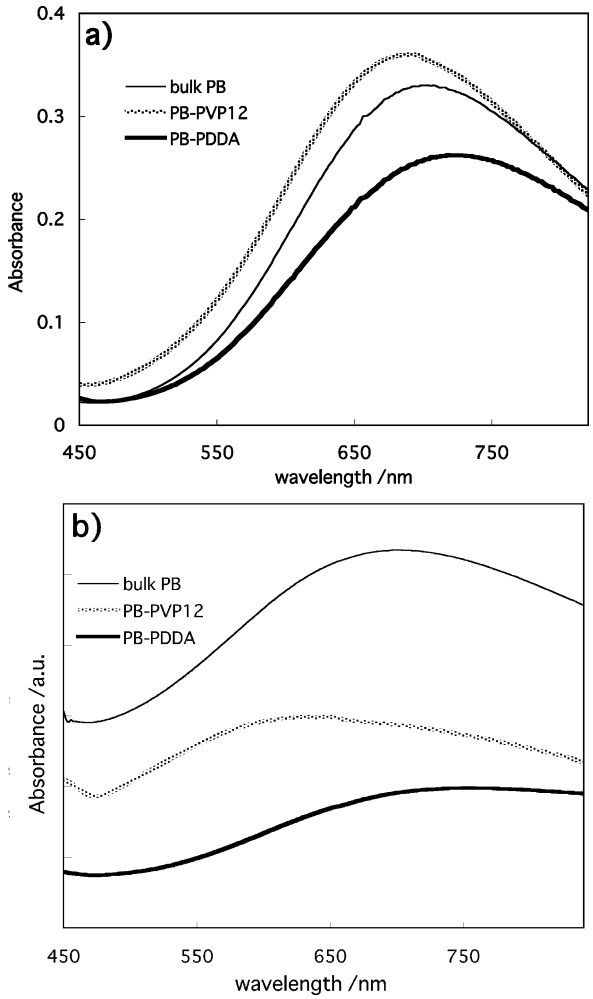


**Figure 5.** UV−vis absorption spectra of bulk PB, PB-PVP27, and PB-PDDA prepared at [$Fe^{2+}$] = 3 mM. [PDDA]/[$Fe^{2+}$] = 100 (a) in aqueous solution and (b) in the solid state.

similar absorption shifts depending on the electronic nature of the bilayers.[14]

Bulk PB is insoluble in organic media, which restricts applications of the molecular magnets as functional materials. The PB-PDDA is also insoluble in organic solvents because of the outer hydrophilic PDDA coating. It is noteworthy that PB-PVP*x* species are soluble in various organic solvents due to the size diminutions and the surface PVP assistance (Figure 6). For example, PB−PVP16 solution in $CHCl_3$ showed the typical broad CT band for PB without any spectral change over one month. TEM images of the sample after evaporation of $CHCl_3$ showed well-dispersed nanoparticles with similar size dimensions (average diameter = 15 nm) compared to the original ones (Figure 7). This result suggests that the surface PVP prevented the inner nanoparticles from further aggregation and dissociation in $CHCl_3$. TEM images of the PB-PVP samples from EtOH also showed the same sphere nanoparticles with maintenance of the nanoparticle size. It is of significance that the supra-

(13) See Supporting Information.

(14) (a) Einaga, Y.; Sato, O.; Iyoda, Y.; Fujishima, A.; Hashimoto, K. *J. Am. Chem. Soc*. **1999**, *121*, 3745. (b) Einaga, Y.; Yamamoto, T.; Sugai, T.; Sato, O. *Chem. Mater*. **2002**, *14*, 4846.

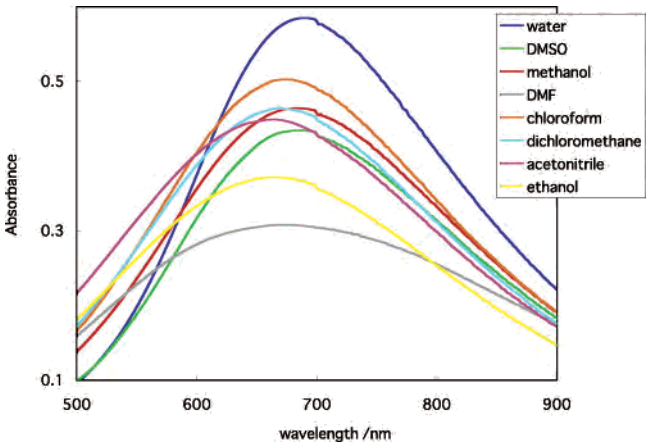


**Figure 6.** UV−vis absorption spectra of PB-PVP12 in various solvents.

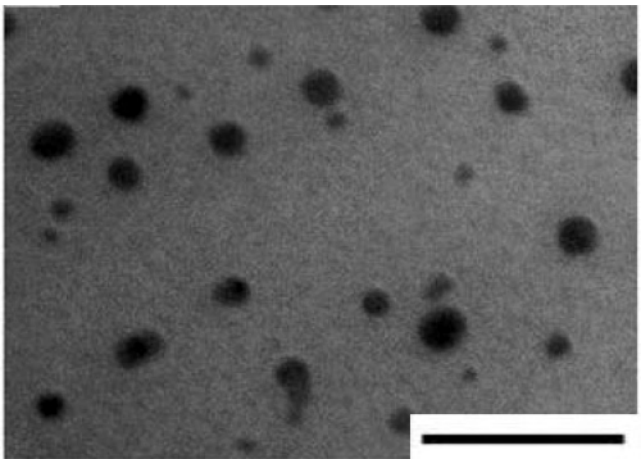

**Figure 7.** TEM image of the sample after evaporation of PB-PVP16 solution in $CHCl_3$. Scale bar = 100 nm.

**Table 1.** Solubilities for PB-PVP12 and Absorption Maxima in the Solutions

| solvent | solubility[a] | $\lambda_{max}$ (nm) |
|---|---|---|
| water | ◎ | 689 |
| DMSO | ◎ | 689 |
| methanol | ◎ | 682 |
| DMF | ○ | 674 |
| chloroform | ○ | 671 |
| dichloromethane | ○ | 668 |
| acetonitrile | △ | 666 |
| ethanol | △ | 663 |

[a] Amount of the solvents required to dissolve 10 mg of PB-PVP12 completely: ◎, less than 0.3 mL; ○, more than 0.3 mL; and △, more than 1.0 mL.

molecular PB keeps the degrees of assembling in the pseudosolution medium.

Table 1 summarizes the absorption maxima and solubilities of PB-PVP16 in the above solvents. From these results, an unprecedented effect of the organic solvents on the optical property of PB was observed. In good solvents for PB-PVP*x* such as water, MeOH, and DMSO, the solvents can easily permeate into the covered PVP. Hence, the interaction between the core PB nanoparticles and the protecting PVP is weak in those media. In relatively poor solvents such as MeCN and EtOH, a solid-state-like environment for the PB nanoparticles is kept, and it leads to the blue shifts of the absorptions because of strong interaction between the PB

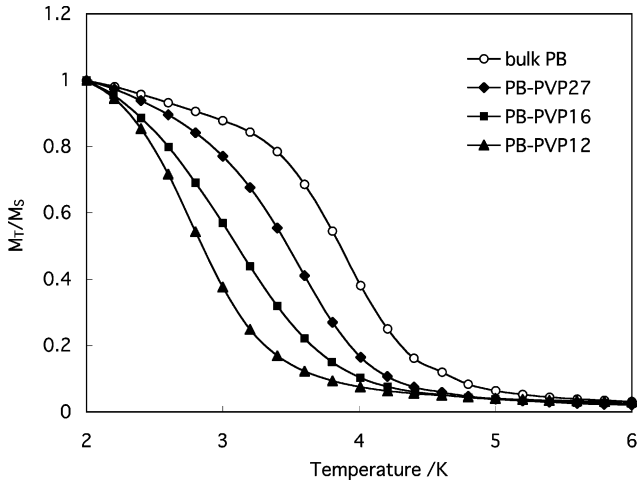


**Figure 8.** Field-cooled magnetization versus temperature curves for PB-PVP27, PB-PVP16, PB-PVP12, and bulk PB at an external magnetic field of 50 G.

nanoparticles and PVP. On the basis of this effect, the surface environments of the PB nanoparticles influence the inherent properties of PB.

**3. Magnetic Properties of the PB Nanoparticles.** The fcc structure of PB allows three-dimensional long-range superexchange interactions between the neighboring $Fe^{3+}$ ions ($S = {}^5/_2$) through the NC−$Fe^{II}$−CN linkages, leading to a ferromagnetic ordering property at low temperature.[7i] Figure 8 shows field-cooled magnetization curves for PB-PVP12, PB-PVP16, PB-PVP27, and bulk PB at an external magnetic field of 50 G. It is recognized that the breaking temperature where PB turns to a ferromagnetic material is related to the particle size of PB. As the particle size becomes smaller, the breaking temperature of PB decreases. This size-dependent feature of the PB particles resulted from an increase of the surface-to-volume ratio with a decrease of the nanoparticle size. For example, the numbers of surface and inner PB unit cells in one nanoparticle of PB-PVP12 are calculated to be approximately 520 and 480, respectively, on the assumption that the nanoparticles are spherical in shape as seen in TEM. In the case of such small nanoparticles, the effect of surface $Fe^{3+}$ moieties having fewer magnetic neighbors than the inner $Fe^{3+}$ ions would strongly affect the magnetic property of PB. Consequently, the diminution of the average number of the nearest magnetic neighbors in the PB nanoparticles lowered the breaking temperature.[5b,15]

The ac magnetization measurements of PB-PVP12, PB-PVP27, and bulk PB were performed (Figure 9a−c). A significant frequency-dependent feature is seen in the profile of nanoPB-PVP12 (Figure 9c). As the particle size of the samples increases, the frequency dependence has not been observed. The magnetic behavior of PB-PVP12 seemed to be superparamagnetism based on nanoparticles with a single magnetic domain.[16] The drop in the magnetization with a

(15) (a) Murray, C. B.; Sun, S.; Doyle, H.; Betly, T. *MRS Bull.* **2001**, 985. (b) Liu, C.; Zhou, B.; Rondinone, A. J.; Zhang, Z. J. *J. Am. Chem. Soc.* **2000**, *122*, 6263.
(16) *Magnetism III*; Rado, G. T., Suhl, H., Eds.; Academic Press: New York, 1963; pp 271−351.

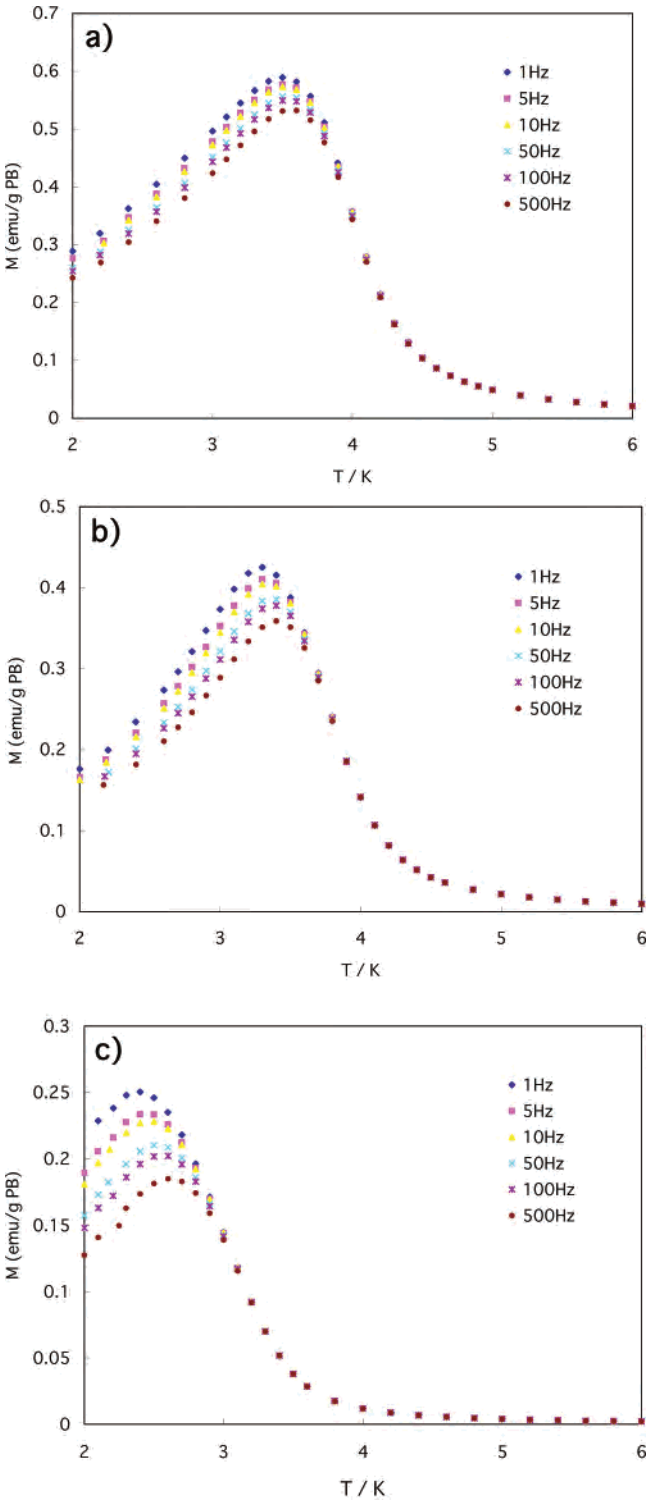


**Figure 9.** Alternating current magnetization profiles of (a) bulk PB, (b) PB-PVP27, and (c) PB-PVP12 at a magnetic field of 3 G.

decrease of the nanoparticle size can be attributed to the increase of less magnetically interacting units at the nanoparticle surfaces. The superparamagnetic behavior of the PB nanoparticles is also supported by field-dependence of magnetization for PB-PVP12 (Figure 10), which shows almost no hysteresis loop,[16] whereas the bulk PB gives distinct hysteresis with a coercive field of approximately 15 G (Figure 10). These results are explained by thermal

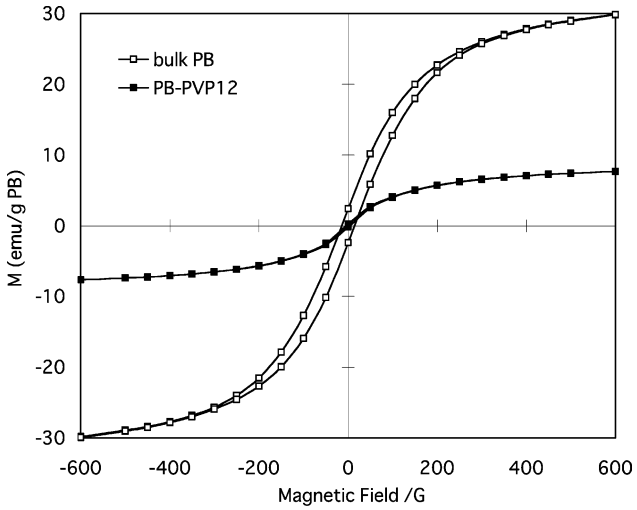


**Figure 10.** Magnetization versus applied magnetic field for bulk PB and PB-PVP12 at 2 K.

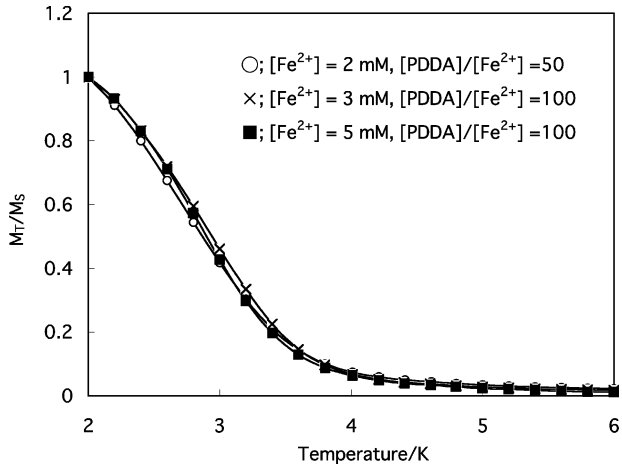


**Figure 11.** Field-cooled magnetization versus temperature curves for PB-PDDA prepared at various synthetic conditions at an external magnetic field of 50 G.

agitations of the nanoparticle magnetic moments. The easily reorienting magnetic moments reduce the coercivity, leading to superparamagnetic-like behavior of the PB nanoparticles.

We also investigated the magnetic properties of PB-PDDA. The field-cooled magnetization measurements of all PB-PDDAs prepared at different conditions gave the same profile with the lower breaking temperature (4.0 K) than that of bulk PB (Figure 11). This result suggests that the sizes of the nanoparticles using the PDDA additive are same at any synthetic conditions, which is consistent with the TEM results. Basically, as is the case of the PVP system, it is expected that PB-PDDA shows the superparamagnetic property due to the very small crystal size. However, the breaking temperature of PB-PDDA is higher than that of PB-PVP12, the ac susceptibility shows small frequency dependence (Figure 12), and the magnetic hysteresis curve has a coercive field of 13 G (Figure 13). This ferromagnetic property is explainable by the CT energy decrease that resulted from the surrounding PDDA. The ease of the CT interaction through the CN bonds enhances the magnetic coupling in PB, leading to the ferromagnetic behavior of PB-PDDA.[14b] From our results, it is demonstrated that the particle

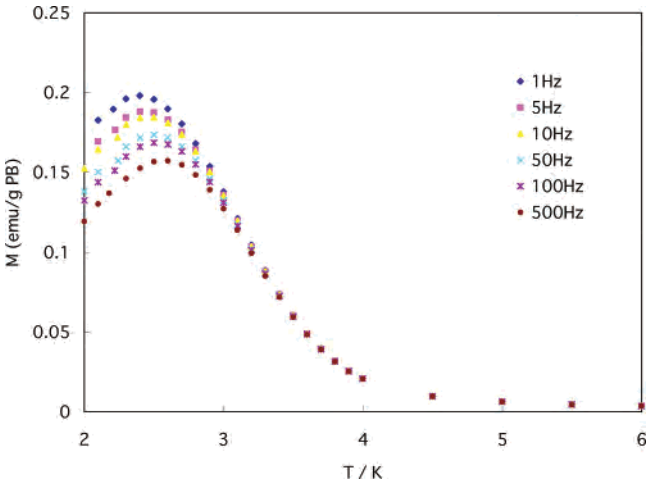


**Figure 12.** (a) Alternating current magnetization profile of PB-PDDA (preparation at $[Fe^{2+}] = 3$ mM, $[PDDA]/[Fe^{2+}] = 100$) at a magnetic field of 3 G.

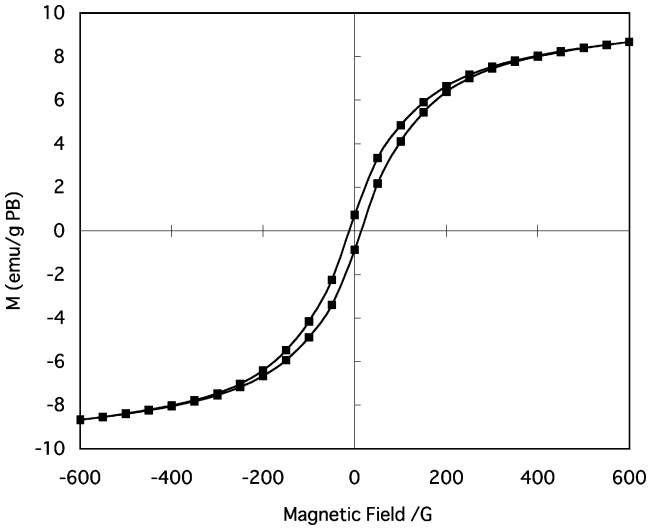


**Figure 13.** Magnetization versus applied magnetic field of PB-PDDA (preparation at $[Fe^{2+}] = 3$ mM, $[PDDA]/[Fe^{2+}] = 100$) at 2 K.

size, as well as the surface protecting polymers, significantly affects the magnetic properties of PB.

## Conclusion

In conclusion, we have succeeded in the facile preparations of the PB nanoparticles protected by organic polymers. The average size of the PB nanoparticles can be finely tuned by choosing organic polymers, concentrations of Fe ions, and feed ratios of Fe to the polymers. A useful technical feature of the present PB nanoparticles is a high processability based on the organic polymer compositions. The surface organic polymers of the PB nanoparticles not only enhance solubilities of PB in organic solvents but also provide film-forming properties when the colloidal dispersions of the composites are evaporated. This work also proved that the inherent properties such as the optical and magnetic characters of PB are significantly modulated by the surface environments and the average size of the PB nanoparticles. The controllable magnetic properties would give valuable information for future applications of the PB family to nanomagnetic materials that attract growing interest because of their potential in ultrahigh-density magnetic recording systems.[17]

**Acknowledgment.** We thank Prof. T. Imanaka and Dr. T. Fukui of Kyoto University for access to TEM. This work was supported by a Grant-in-Aid for Scientific Research in a Priority Area "Chemistry of Coordination Space" and by "Nanotechnology Support Project" of the Ministry of Education, Culture, Sports, Science and Technology, Japan. T.U. appreciates Mitsubishi Chemical Corporation Fund for financial support.

**Supporting Information Available:** Size histograms of the PB nanoparticles, XRPD pattern, and IR spectrum of PB-PDDA (PDF). This material is available free of charge via the Internet at http://pubs.acs.org.

IC0488435

(17) (a) Black, C. T.; Murray, C. B.; Sandstrom, R. L.; Sun, S. *Science* **2000**, *290*, 1131. (b) Sun, S.; Murray, C. B.; Weller, D.; Folks, L.; Moser, A. *Science* **2000**, *287*, 1989. (c) Hashimoto, S.; Maesaka, A.; Fujimoto, K.; Bessho, K. *J. Magn. Magn. Mater*. **1993**, *121*, 471.